Oxidation of ZrB$_2$- and HfB$_2$-based ultra-high temperature ceramics: Effect of Ta additions

E. OPILA, S. LEVINE
NASA Glenn Research Center, Brookpark, OH 44135, USA
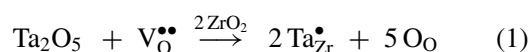*E-mail: Elizabeth.J.Opila@grc.nasa.gov*

J. LORINCZ
Ohio University, Athens, OH 45701, USA

Several compositions of ZrB$_2$- and HfB$_2$-based Ultra-High Temperature Ceramics (UHTC) were oxidized in stagnant air at 1627°C in ten minute cycles for times up to 100 min. These compositions include: ZrB$_2$-20 vol% SiC, HfB$_2$-20 vol% SiC, ZrB$_2$-20 vol% SiC-20 vol% TaSi$_2$, ZrB$_2$-33 vol% SiC, HfB$_2$-20 vol% SiC-20 vol% TaSi$_2$, and ZrB$_2$-20 vol% SiC-20 vol% TaC. The weight change due to oxidation was recorded. The ZrB$_2$-20 vol% SiC-20 vol% TaSi$_2$ composition was also oxidized in stagnant air at 1927°C and in an arc jet atmosphere. Samples were analyzed after oxidation by X-ray diffraction, field emission scanning electron microscopy, and energy dispersive spectroscopy to determine the reaction products and to observe the microstructure. The ZrB$_2$-20 vol% SiC-20 vol% TaSi$_2$ showed the lowest oxidation rate at 1627°C, but performed poorly under the more extreme tests due to liquid phase formation. Effects of Ta-additions on the oxidation of the diboride-based UHTC are discussed. © *2004 Kluwer Academic Publishers*

1. Introduction

Preliminary results for the oxidation of ZrB$_2$-20 vol% SiC-20 vol% TaSi$_2$ [1] showed improved oxidation resistance relative to the baseline material ZrB$_2$-20 vol% SiC. This improved behavior was attributed to the addition of Ta to the system. One possibility for the improved oxidation resistance, explored by Talmy *et al.* [2], is that Ta$_2$O$_5$ in the borosilicate glass causes liquid immiscibility and phase-separated glasses of higher viscosity and lower permeability to oxygen. Talmy *et al.* found TaB$_2$ additions to ZrB$_2$-20 v/o SiC were more effective in improving oxidation resistance at temperatures between 1200 and 1400°C than additions of other group IV–VI transition metal borides, including Cr, Nb, Ti, and V. No significant improvement in oxidation resistance at temperatures of 1500°C was found for any additions.

Another possible explanation for this improved behavior is that Ta additions result in substitution of Ta on the Zr site in ZrO$_2$, reducing the concentration of oxygen vacancies in the ZrO$_2$ per the following doping reaction given in standard Kroger-Vink notation:

$$\text{Ta}_2\text{O}_5 \; + \; \text{V}_\text{O}^{\bullet\bullet} \; \xrightarrow{2\,\text{ZrO}_2} \; 2\,\text{Ta}_\text{Zr}^\bullet \; + \; 5\,\text{O}_\text{O} \qquad (1)$$

The resultant lower concentration of oxygen vacancies decreases oxygen transport through the growing oxide scale, and thus lowers the oxidation rate of tantalum-containing UHTC materials. There is some precedence for Ta$_2$O$_5$ acting as a vacancy suppressor in ZrO$_2$-based materials [3, 4]. Ionic conductivity in 90 m/o ZrO$_2$-10 m/o Y$_2$O$_3$ decreased with Ta$_2$O$_5$ additions up to 10

mol% [4]. Greater Ta$_2$O$_5$ additions did not result in any further decrease in ionic conductivity.

The purpose of this work is to explore effects of Ta-additions to UHTC in hopes of improving oxidation properties for this class of materials to enable their use in space transportation leading edge applications for short times at very high temperatures. This paper represents a preliminary investigation on the oxidation resistance of Ta-containing UHTC.

2. Experimental procedure

ZrB$_2$- and HfB$_2$-based UHTC were prepared from powders described in Table I. Six compositions, their designation, and processing history are summarized in Table II. The powders were mixed, and then milled using Si$_3$N$_4$ media in hexane in a Si$_3$N$_4$ mill for 24 h. The powders were vacuum hot pressed using a graphite die. Further details can be found in reference [1].

Sample coupons of 2.5 cm × 1.2 cm × 0.3 cm were machined from hot pressed plates. The coupons were ultrasonically cleaned in detergent (Micro-90, International Products Corporation), de-ionized water, acetone, and alcohol prior to oxidation. X-ray diffraction and Energy Dispersive Spectroscopy of as-machined and cleaned coupons indicated the desired phase assemblage was formed in all cases except the ZSTS and ZSTC material. Analysis indicated ZSTS contained ZrB$_2$, SiC, TaSi$_2$ and possibly a minor amount of a (Zr, Ta) boride solution. ZSTC contained ZrB$_2$, SiC, and (Zr, Ta) boride and carbide solution phases. Initial surface areas and sample weights were recorded.

ULTRA-HIGH TEMPERATURE CERAMICS

TABLE I Powders used for UHTC sample preparation

Material	Source	Particle size	Purity (%)
ZrB_2	Cerac	$<10\ \mu m$	99.5
HfB_2	Cerac	-325 mesh	99.5
SiC	H.C. Starck	$<5\ \mu m$	>99.9
$TaSi_2$	Cerac	$80\%\ -325$ mesh	>99.9
TaC	Cerac	-325 mesh	99.5

TABLE II Summary of UHTC compositions, designations, and processing

Composition	Designation: oxidation temp.	Processing	Density (g/cm^3)	Density $(\%)^a$
ZrB_2-20 vol% SiC	ZS	2000°C, 10 ksi, 2 h	5.27	95.5
HfB_2-20 vol% SiC	HS	2000°C, 10 ksi, 2 h	9.60	97.0
ZrB_2-20 vol% SiC-20 vol% $TaSi_2$	ZSTS: 1627°C	1600°C, 10 ksi, 2 h	5.92	97.7
ZrB_2-20 vol% SiC-20 vol% $TaSi_2$	ZSTS: 1927°C	1600°C, 10 ksi, 2 h	6.04	99.7
ZrB_2-33 vol% SiC	ZS+	2000°C, 10 ksi, 2 h	5.04	97.5
ZrB_2-20 vol% SiC-20 vol% TaC	ZSTC	2000°C, 10 ksi, 2 h	7.12	98.9
HfB_2-20 vol% SiC-20 vol% $TaSi_2$	HSTS	1700°C, 10 ksi, 2 h	9.13	100.0

^{a}Based on rule-of-mixtures.

TABLE III XRD results and parabolic oxidation rates for UHTC materials oxidized in air at 1627°C. XRD results in bold indicate major phases present

Composition	Designation	XRD results	k_p (mg^2/cm^4h)
ZrB_2-20 vol% SiC	ZS	**ZrO_2(m)**, ZrO_2(c)	10.94
HfB_2-20 vol% SiC	HS	**HfO_2(m)**	2.52
ZrB_2-20 vol% SiC-20 vol% $TaSi_2$	ZSTS	**ZrO_2(m)**, ZrO_2(c)	0.29
ZrB_2-33 vol% SiC	ZS+	**ZrO_2(m)**, ZrO_2(c)	NA
ZrB_2-20 vol% SiC-20 vol% TaC	ZSTC	**ZrO_2(t)**, ZrO_2(m)	NA
HfB_2-20 vol% SiC-20 vol% $TaSi_2$	HSTS	**HfO_2(m)**, **HfO_2(c)**, **$HfSiO_4$**	5.73

(m) = monoclinic, (c) = cubic, (t) = tetragonal.

Samples were oxidized at 1627°C in stagnant air in bottom loading box furnaces, either a DelTech, Inc. zirconia element furnace or a CM Inc. $MoSi_2$ element furnace. Oxidation of ZrB_2-20 vol% SiC-20 vol% $TaSi_2$ was also conducted in the DelTech zirconia element furnace at 1927°C. Three coupons were loaded into a slotted calcia-stabilized zirconia firebrick setter (98.7% purity). Two lines of contact existed between the setter and sample. The coupons were oxidized for ten minute cycles. A coupon was removed after one cycle, five cycles, and ten cycles. A maximum oxidation time of 100 min was achieved. Post-oxidation weight changes were recorded where possible. Some coupons stuck to the zirconia setter due to extensive glass formation. Optical macrographs were taken of all coupons after oxidation. The sample surfaces were analyzed by X-ray Diffraction (XRD), Field Emission Scanning Electron Microscopy (FESEM), and Energy Dispersive Spec-troscopy (EDS) to determine phases present before and after oxidation as well as oxide microstructures. Several materials were also examined by FESEM and EDS in cross-sections that were prepared by non-aqueous cutting and polishing procedures.

The ZrB_2-20 vol% SiC-20 vol% $TaSi_2$ composition was also tested in an arc jet in the Interactive Heating Facility at NASA Ames Research Center. Details can be found in Reference [5]. The sample reached temperatures between 1800 and 1960°C in a 10 minute exposure at a stagnation pressure of 0.07 atm and a nominal heat flux of 350 W/cm^2.

3. Results
3.1. Oxidation at 1627°C in air
Macrographs of the coupons after oxidation are shown in Fig. 1a through f. X-ray diffraction results are summarized in Table III. In all cases, ZrO_2 or HfO_2 was the major phase detected on ZrB_2- and HfB_2-based materials respectively. $HfSiO_4$ was only detected on HSTS.

Plots of the specific weight change vs. oxidation time for coupons exposed at 1627°C in stagnant air are shown in Fig. 2. All compositions except ZSTC showed evidence of the formation of a protective scale, that is, the oxidation rate slowed with time. The results for the remaining compositions are plotted as specific weight change versus square root of time in Fig. 3. The fit of the data to a straight line on this type of plot indicates parabolic oxidation, that is, the oxidation rate is limited by transport of oxidant across the growing oxide scale. The slope of such a line is equivalent to the square root of the parabolic rate constant, k_p. From Fig. 3, it can be seen that the results for ZS, HS, ZSTS, and HSTS show reasonably good fits to parabolic kinetics. Parabolic rate constants are reported in Table III for these four compositions. While these numbers can be used to make semi-quantitative comparisons of oxidation rate, they are not strictly comparable because different compositions of reaction products form on each sample type. A more quantitative comparison will be made in future reports by comparing rate constants derived from recession vs. time measured from cross-sections of oxidized samples.

FESEM results are shown in Figs 4 through 7. Figs 4 and 5 show the cross-section of oxidized ZS baseline material and ZSTS respectively. Note the much thinner oxide scale on the ZSTS material which is consistent with the low oxidation rate as measured by weight change. Porosity, due to SiC depletion by active oxidation, is observed near the oxide/matrix interface for the ZS material shown in Fig. 4. Fig. 6 shows a surface micrograph of ZSTS. Note the evidence of glass immiscibility. EDS indicates the phase of medium contrast contains Al and Mg impurities. It is not clear that any Ta is present in the glass phases. EDS indicates that Ta may be present in the ZrO_2 phase, however, this must be confirmed by another analytical technique. Fig. 7 shows a surface micrograph of the ZSTC material. The porosity in the oxide scale is clearly visible. The non-protective nature of this oxide scale is
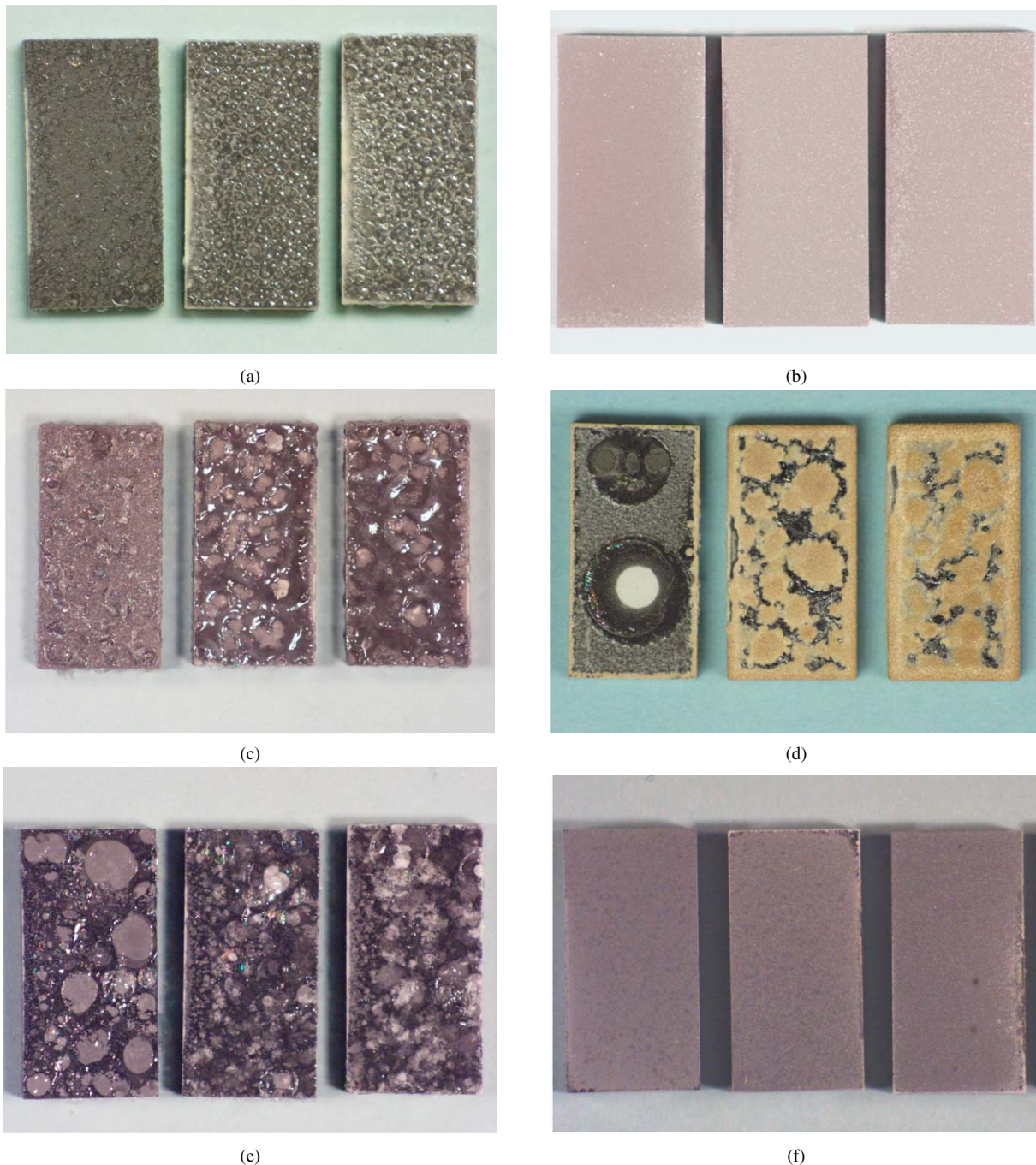
Figure 1 UHTC oxidized at 1627°C in air for 1, 5, and 10 ten-minute cycles: (a) ZS, (b) ZSTS, (c) ZS+, (d) ZSTC, (e) HS, and (f) HSTS.

consistent with the observed rapid linear weight change kinetics.

3.2. Oxidation at 1927°C

Macrographs of the ZSTS coupons after oxidation at 1927°C in stagnant air are shown in Fig. 8. After five oxidation cycles, the samples were bonded to the setter by liquid oxide phase formation. Weight change measurements were not possible. Fig. 8c was taken after the sample was broken during an attempt to remove the coupon from the setter. The cross-section shows a gap between the scale and the substrate, showing that rapid substrate consumption occurred. XRD of the oxide scale showed monoclinic ZrO_2 as the major phase

and cubic ZrO_2 as a minor phase. XRD of the substrate with the scale removed gave the same results. In contrast, evidence of Ta_2O_5 as well as possible zirconium tantalate formation on the substrate below the ZrO_2 scale was found by EDS analysis as shown in Fig. 9. However, this identification is complicated by the fact that the Ta M_α peak (1.709 keV) has almost complete overlap with the Si K_α peak (1.739 keV). Ta identification was made primarily by observing the low intensity Ta L_α peak at 8.145 keV. In addition, phases with high Si content would have much darker contrast than those with high Ta content. Wavelength dispersive spectroscopy (WDS) is planned to address the peak overlap problem as well as to resolve the discrepancy between XRD and EDS results. Fig. 10 shows FESEM images of
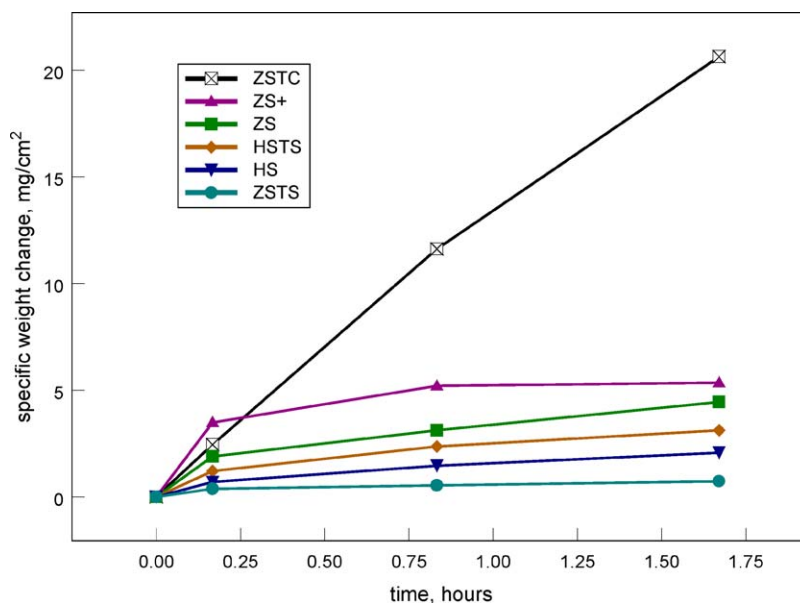
Figure 2 Specific weight change for all UHTC compositions oxidized at 1627°C in air.
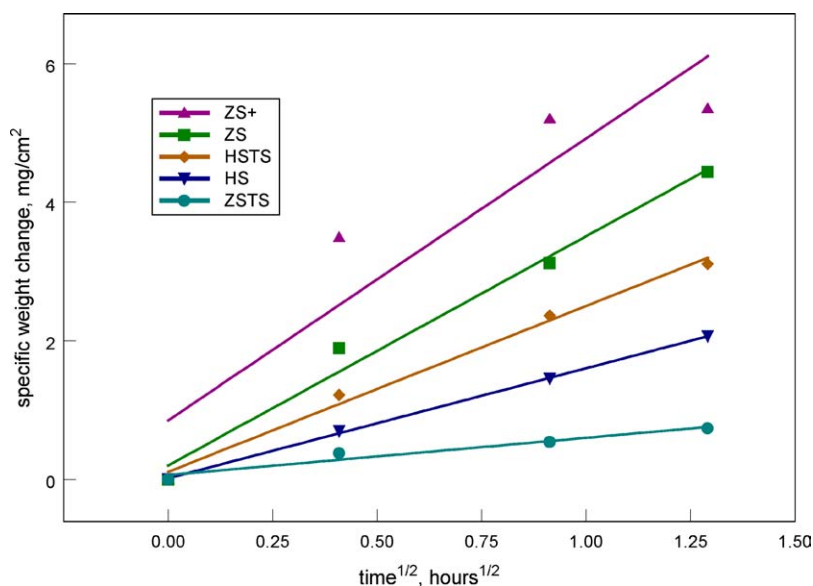

Figure 3 Fit of specific weight change data to parabolic kinetics for UHTC compositions with SiC additions indicating protective oxide formation at 1627°C in air, however, ZS+ does not show good agreement with parabolic kinetics.

the oxide scale outer surface as well as the underside of the intact oxide scale that was removed. The dark silica-containing phase is observed on the outer surface but only in much smaller amounts on the underside of the oxide. The bright phases on both the outer and underside of the scale were identified as ZrO_2 and zirconium tantalate.

3.3. Arc jet testing
Fig. 11 shows a macrograph of the 2.54 cm diameter button of ZSTS after arc jet exposure for 10 min. The scale composition and morphology are similar to that observed after oxidation at 1927°C (Fig. 10, left). Again, evidence of liquid phase formation is observed. Similarly, Ta_2O_5 was tentatively identified below the oxide scale by EDS [4].

4. Discussion
A comparison of the oxidation rate of the ZS and ZSTS compositions at 1627°C in air clearly showed the benefit of $TaSi_2$ additions toward improving the oxidation resistance of ZrB_2-based UHTC materials [1]. These initial results led to a series of questions that we have answered to varying degrees by the work described here.

4.1. Is Ta or Si in $TaSi_2$ responsible for the improved oxidation resistance of ZSTS?
The ZS+ composition was fabricated to answer this question. The ZS+ composition contains the same amount of ZrB_2 as ZSTS and the same amount of Si (in the form of SiC) as ZSTS. If the increased oxidation resistance of ZSTS relative to ZS was due to the increased amount of Si, and therefore more SiO_2
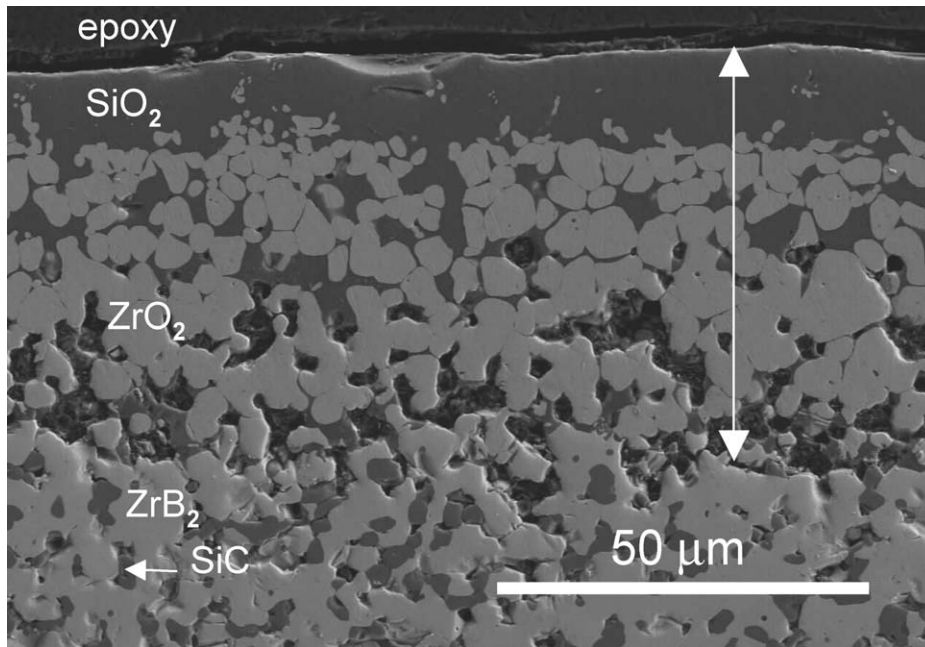
Figure 4 ZS cross-section after oxidation in air at 1627°C for 100 min. Arrow shows oxide thickness. Representative areas of each phase are labeled.
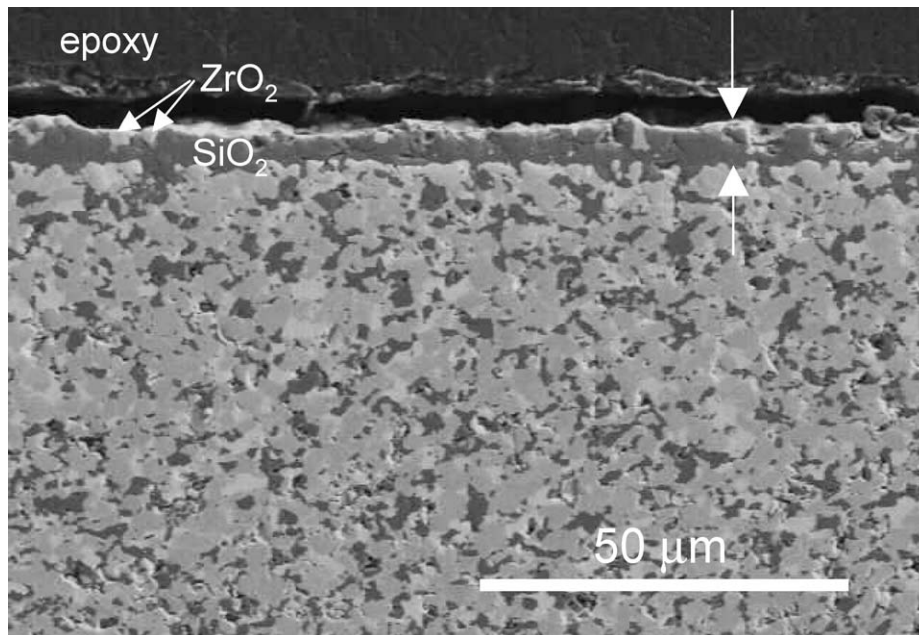

Figure 5 ZSTS cross-section after oxidation in air at 1627°C for 100 min. Arrows show oxide thickness. Representative areas of each oxide phase are labeled. The unoxidized ZSTS below the scale contains three contrasting phases: dark SiC; medium ZrB_2 and $(Zr, Ta)B_2$, bright $TaSi_2$.

formation on oxidation, then it is expected that ZS+ would have oxidation resistance superior to that of ZS. In fact, the opposite occurred. Fig. 1c shows the increased glass formation of this material, while Fig. 2 shows the ZS+ has a higher oxidation rate than both ZS and ZSTS. This result supports the conclusion that Ta additions are responsible for improving the oxidation resistance of ZrB_2-based materials.

4.2. Does the benefit of $TaSi_2$ additions observed at 1627°C extend to higher temperatures?

Clearly the $TaSi_2$ additions to ZS did not provide superior oxidation resistance at temperatures near 1900°C,

but in fact the opposite. Liquid phases were formed in both the 1927°C furnace oxidation and the arc jet tests. This can be expected based on the phase diagram for the ZrO_2-Ta_2O_5 system [6]. The melting point of Ta_2O_5 is 1785°C for the low-temperature phase and 1872°C for the high-temperature phase [7]. The observed liquid could be due to melting of Ta_2O_5. However, a zirconium tantalate phase, called phase V, may also be responsible for this liquid phase formation. Phase V is of variable composition and has been described as $Ta_2O_5 \cdot 6ZrO_2$ [8], $Ta_2O_5 \cdot 5.5\, ZrO_2$ [9], or containing 11 to 17% Ta_2O_5 in ZrO_2 [10]. The melting point of phase V is uncertain and has only been defined to be higher than 1870°C [8]. It is difficult to unambiguously distinguish phase V from cubic zirconia by XRD. The introduction of
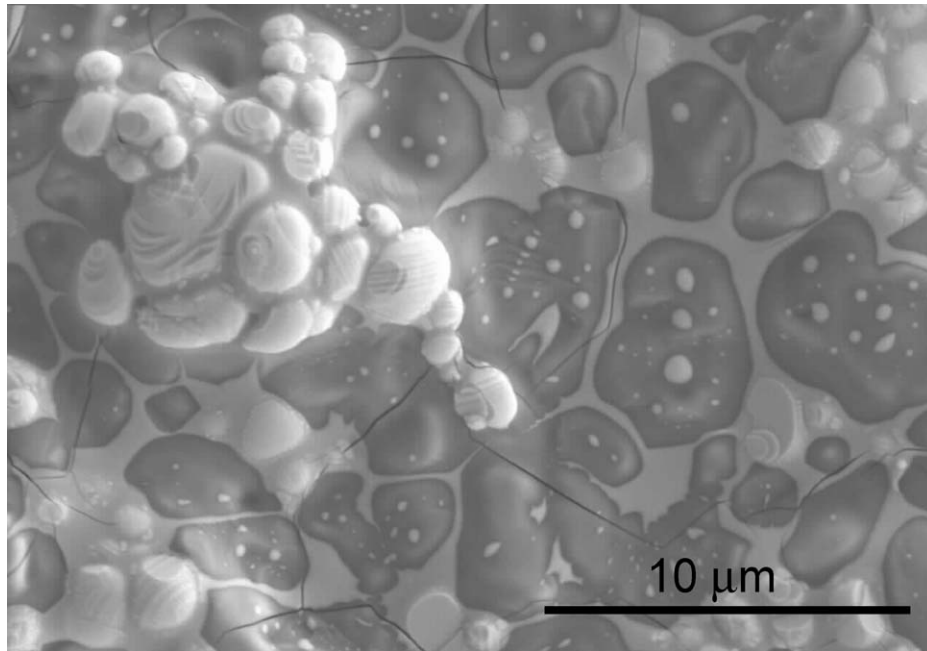
Figure 6 Surface morphology of ZSTS after oxidation in air at 1627°C for 100 min showing evidence of glass immiscibility. Bright phase, ZrO_2; medium phase, silicate glass with impurities; dark phase, SiO_2.
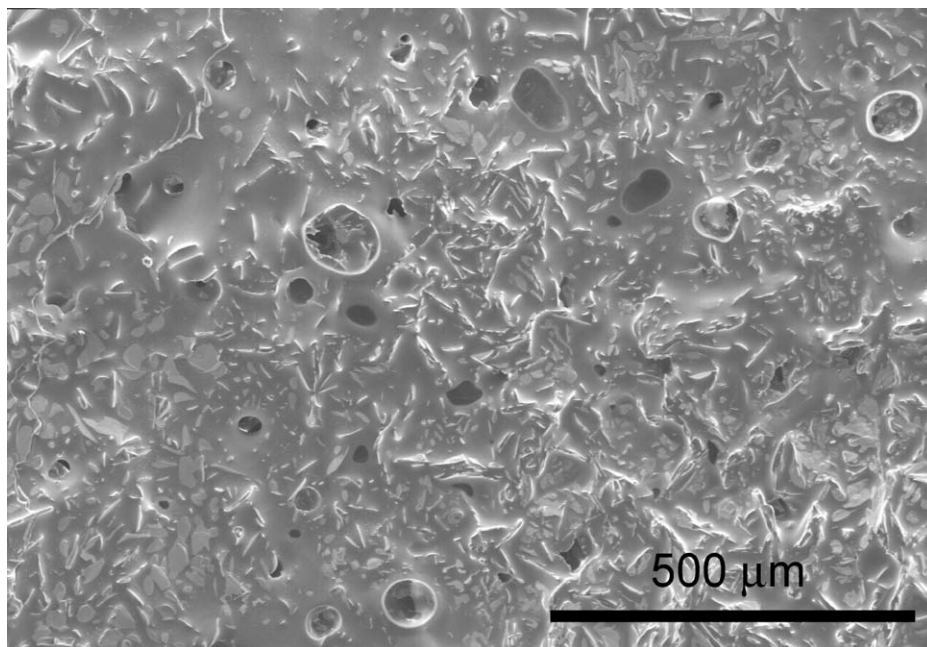

Figure 7 Surface morphology of ZSTC after oxidation in air at 1627°C for 100 min.
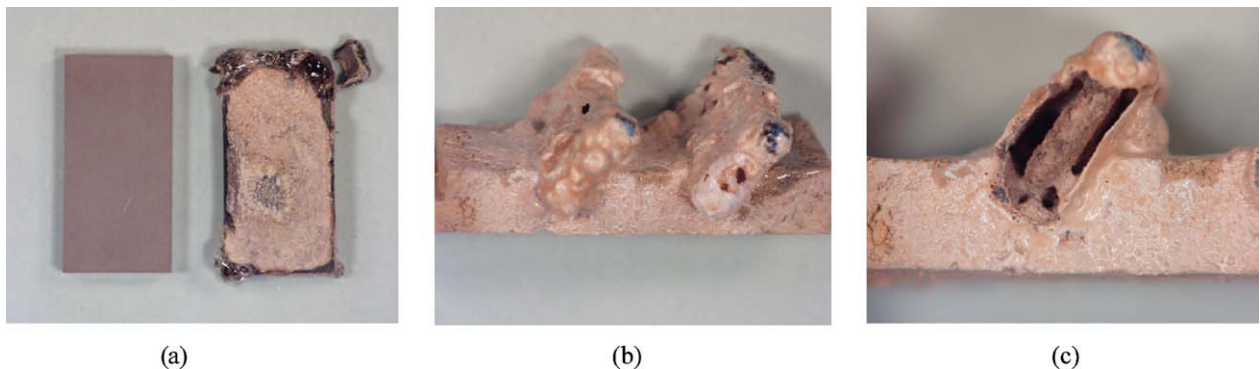

Figure 8 ZSTS after oxidation at 1927°C in stagnant air: (a) as-received and 1 cycle, (b) 5 ten-min cycles in setter, and (c) 5 ten-min cycles.
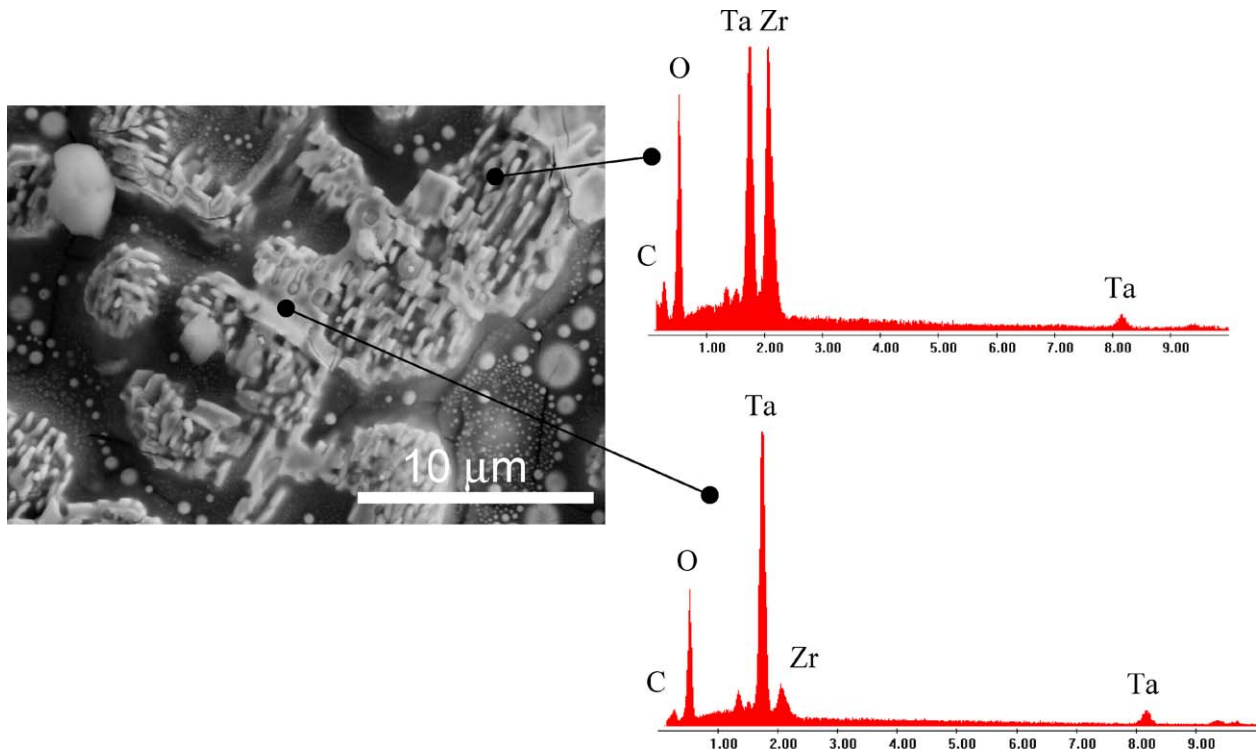
Figure 9 ZSTS substrate (loose scale has been removed) after exposure in stagnant air at 1927°C for 5 ten-min cycles. EDS results on flatter regions of the bright phase are consistent with Ta_2O_5, while EDS on the bright thin aligned grains is consistent with zirconium tantalate. The dark phase is identified as SiO_2 (EDS not shown).
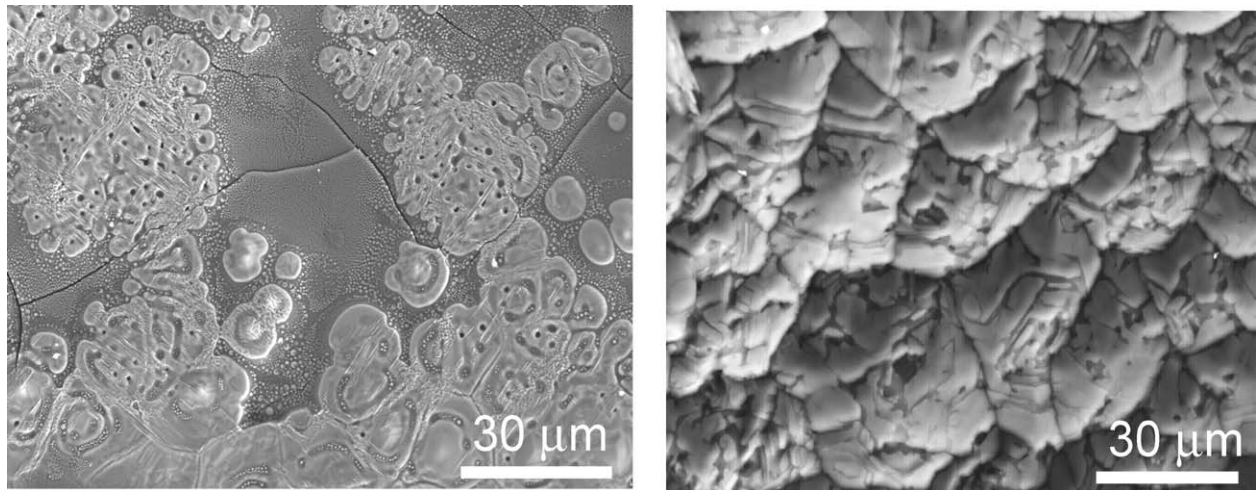

Figure 10 ZSTS outer scale removed after exposure in stagnant air at 1927°C for 5 ten-min cycles. Left: outer surface of scale. Dark phase is SiO_2, bright phase ZrO_2 and Zr-Ta-O. Right: underside of scale showing less SiO_2.

Ta_2O_5 into the cubic zirconia structure to form phase V results in a distorted orthorhombic structure [9] with all lattice parameters close to those of cubic zirconia. Clearly, Ta_2O_5 and possible excessive amounts of the phase V should be avoided. If Ta_2O_5 is present only in solution with ZrO_2, this would be avoided. The extent of Ta_2O_5 solubility in ZrO_2 is unknown, but some solubility is likely since the Ta^{+5} and Zr^{+4} ions are of similar size (0.73 vs. 0.80 angstroms). A phase diagram for the related system ZrO_2-Nb_2O_5 system [10] shows 5 to 10 mol% solubility of Nb_2O_5 in ZrO_2. Currently, compositions with 5 vol% $TaSi_2$ are being fabricated in hopes of avoiding liquid phase formation at ultra-high temperatures. Oxidation of this new material at 1927°C is planned.

4.3. Are $TaSi_2$ additions the best way to add Ta to ZrB_2-based UHTC?

The ZSTC (TaC additions to ZrB_2-SiC) composition was formulated specifically to address this issue. Other possible vehicles for Ta additions include TaB_2 and Ta_5Si_3. A composition with 20 v/o TaC addition was chosen to see if the Ta additions offered improvements without additional B_2O_3 or SiO_2 glass formation. As previously mentioned, the oxidation kinetics for ZSTC at 1627°C were rapid and linear indicating non-protective oxide formation, presumably due to scale porosity formed by evolution of CO and/or CO_2 during the oxidation process. Results were not only much worse than the ZSTS composition, but also worse than the baseline ZS material. This is consistent
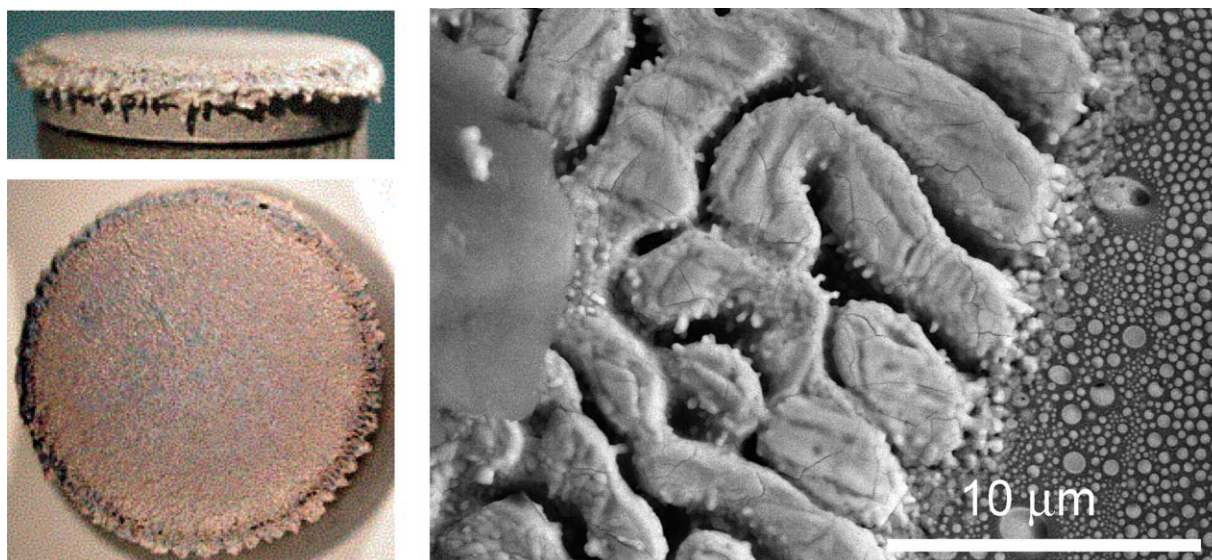
Figure 11 ZSTS after testing in an arc jet at approximately 1890°C for ten min. Left: macro photos of 2.5 cm button. Right: surface oxide showing evidence of melting.

with previous results obtained for the HfB$_2$-HfC system at 1500°C in air [11]. Protective scales were formed on HfB$_2$ at 1500°C. The scales became less protective as HfC was substituted for HfB$_2$, with the most rapid oxidation for pure HfC. However, at the ultra-high temperatures achieved in arc jet testing, the HfC performed better than HfB$_2$. The better ultra-high temperature behavior of HfC was attributed to the tendency for the gaseous oxidation products CO and/or CO$_2$ to be less disruptive to the HfO$_2$ scale than boiling B$_2$O$_3$. Oxidation of the ZSTC composition at 1927°C is planned to further evaluate this concept.

4.4. Can TaSi$_2$ additions improve the oxidation resistance of HfB$_2$-based UHTC which are already superior to ZrB$_2$-based materials?

Oxidation resistance of the HS material was not improved, but actually worsened, by 20 v/o addition of TaSi$_2$. The HfO$_2$-Ta$_2$O$_5$ system appears to be even less studied than the corresponding ZrO$_2$ system. However, there is evidence that the systems are similar in several respects. Some solid solution of the two oxide phases, as well as formation of a Ta$_2$O$_5$·6HfO$_2$ phase, were both observed [12]. However, differences in oxidation rates of Hf metal and Zr metal have been documented. The parabolic oxidation rate constant of Hf metal has the same activation energy as that of Zr metal, indicating the transport of oxidant through HfO$_2$ occurs by the same mechanism as that in ZrO$_2$; however, the pre-exponential is lower indicating a lower number of defects available for oxygen transport in HfO$_2$ [13]. Ta-additions may be less effective in HfO$_2$ than in ZrO$_2$ due to this possible difference in oxygen vacancy concentration.

Another difference in the Zr-based and Hf-based SiC-containing UHTC is the upper temperature stability limit of ZrSiO$_4$ versus HfSiO$_4$. The decomposition temperature of ZrSiO$_4$ is not particularly well known.

ZrSiO$_4$ decomposes to form ZrO$_2$ and SiO$_2$ at temperatures reported as low as 1538°C [14] or as high as 1676°C [15]. The XRD results from this study showed the absence of the ZrSiO$_4$ phase for ZSTS after oxidation at 1627°C, consistent with the lower value of the ZrSiO$_4$ stability temperature limit. The upper stability temperature of HfSiO$_4$ appears to be higher than for ZrSiO$_4$ although it is even less well studied. The only phase diagram found indicates HfSiO$_4$ melts incongruently at 1750°C [16]. HfSiO$_4$ was observed by XRD on HSTS after oxidation at 1627°C. The presence or absence of this MSiO$_4$ phase may influence the oxidation kinetics. The oxygen transport rate in these MSiO$_4$ phases is expected to be lower than in the respective MO$_2$ oxides [17]. The oxidation rate for the HSTS material, which formed HfSiO$_4$, was higher than that of the ZSTS, which did not form ZrSiO$_4$. These results are inconsistent with a mechanism of reduced oxygen transport due to formation of an MSiO$_4$ phase.

The oxidized HSTS has not yet been analyzed microstructurally. Any differences in the oxide morphology and composition between the oxidized HS, HSTS and ZSTS materials will allow a better understanding of the effects of Ta-additions to the HS system. This microstructural work is also planned.

4.5. Can anything be learned about the mechanism by which Ta-additions improve the oxidation resistance of ZS materials at 1627°C?

More work is needed to answer this question. While glass immiscibility was observed for the ZSTS material after oxidation at 1627°C, it was not clear that tantalum was present in either of the phase-separated glasses. The phase identity and composition of the crystalline oxidation products remains uncertain due to energy overlaps in EDS Ta and Si peaks and similarity of XRD patterns for ZrO$_2$(c) and Ta$_2$O$_5$·6ZrO$_2$. Electron microprobe and/or WDS are needed to better characterize the oxidation products.

5. Summary and conclusions

The addition of 20 v/o $TaSi_2$ to ZrB_2-SiC clearly improves the oxidation resistance of this material at $1627°C$ in air. The improved behavior is attributed to effects of Ta, not Si, although the mechanism for this improvement is not yet understood. Liquid phase formation due to melting of either Ta_2O_5 or $Ta_2O_5·6ZrO_2$ at $1927°C$ is a problem for the material with 20 v/o $TaSi_2$ in ZrB_2-SiC. TaC additions are not effective in improving the oxidation resistance of ZrB_2-SiC at $1627°C$. The addition of $TaSi_2$ to the HfB_2-SiC system does not increase the oxidation resistance of this material at $1627°C$ in air.

Future work includes the following: Measure the recession due to oxidation of UHTC materials to better quantify their oxidation rates. Characterize the oxidation products using WDS to better understand the amounts and compositions of phases present. Fabricate, oxidize and analyze UHTC materials with 5 v/o $TaSi_2$ additions in hopes of avoiding liquid phase formation at temperatures greater than the melting point of Ta_2O_5 and $Ta_2O_5·6ZrO_2$. Continue to examine other compounds as vehicles for Ta-additions to UHTC.

Acknowledgments

References

1. S. R. LEVINE and E. J. OPILA, "Tantalum Addition to Zirconium Diboride for Improved Oxidation Resistance," NASA/TM—2003-212483 (2003).
2. I. G. TALMY, J. A. ZAYKOSKI, M. M. OPEKA and S. DALLEK, "Oxidation of ZrB_2 Ceramics Modified with SiC and Group IV-VI Transition Metal Borides," in High Temperature Corrosion and Materials Chemistry III, edited by M. McNallan and E. Opila (The Electrochemical Society, Inc., Pennington, NJ, 2001) p. 144.
3. M. CAILLET, C. DEPORTES, G. ROBERT, G. VALLIER and G. VITTER, *Rev. Int. Haute Temper. et Refract.* **5** (1968) 173.
4. A. G. KOTLYAR, A. D. NEUIMIN, S. F. PAL'GUEV, V. N. STREKALOVSKII and V. N. ZUBANKOV, *Inorg. Mater.* **6**(2) (1970) 281.
5. S. R. LEVINE, M. SINGH, E. J. OPILA, J. A. LORINCZ, J. PETKO, D. T. ELLERBY and M. J. GASCH, "Ultra-High Temperature Ceramic Composites for Leading Edges," JANNAF 39th Combustion/27th Airbreathing Propulsion/21st Propulsion Systems Hazards/3rd Modeling and Simulation Joint Subcommittee Meeting, Colorado Springs, Dec. 1–5, 2003.
6. E. M. LEVIN, C. R. ROBBINS and H. F. MCMURDIE, "Phase Diagrams for Ceramists" (The American Ceramic Society, Inc., Columbus, OH, 1964) p. 144.
7. A. REISMAN, F. HOLTZBERG, M. BERKENBILT and M. BERRY, *J. Amer. Chem. Soc.* **78** (1956) 4514.
8. B. W. KING, J. SCHULTZ, E. A. DURBIN and W. H. DUCKWORTH, "Some Properties of Tantala Systems," Battelle Memorial Institute Report No. BMI-1106, 1956.
9. Powder Diffraction File, International Centre for Diffraction Data, Swarthmore, Pennsylvania, card no. 42–60.
10. "Phase Diagrams for Zirconium and Zirconia Systems", edited by H. M. Ondik and H. F. McMurdie (The American Ceramic Society, Westerville, OH, 1998) p. 144.
11. A. G. METCALFE, N. B. ELSNER, D. T. ALLEN, E. WUCHINA, M. OPEKA and E. OPILA, "Oxidation of Hafnium Boride," in "High Temperature Corrosion and Materials Chemistry," edited by M. McNallan, E. Opila, T. Maruyama and T. Narita (The Electrochemical Society Inc., Pennington, NJ, 2000) p. 489.
12. R. L. MAGUNOV and I. R. MAGUNOV, *Functional Mater.* **8**(3) (2001) 560.
13. P. KOFSTAD, "High Temperature Corrosion" (Elsevier Science Publishing Company, New York, 1988) p. 307.
14. C. E. CURTIS and H. G. SOWMAN, *J. Amer. Ceram. Soc.* **36**(6) (1953) 190.
15. W. C. BUTTERMAN and W. R. FOSTER, *Amer. Mineral.* **52**(5/6) (1967) 880.
16. E. M. LEVIN and H. F. MCMURDIE, "Phase Diagrams for Ceramists, 1975 Supplement" (The American Ceramic Society, Inc., Columbus, OH, 1975) p. 165.
17. E. L. COURTRIGHT, J. T. PRATER, C. H. HENAGER and E. N. GREENWELL, "Oxygen Permeability for Selected Ceramic Oxides in the Range 1200°C–1700°C," WL-TR-91-4006 (1991).